

## Magnetic phase evolution in the $\text{LaMn}_{1-x}\text{Fe}_x\text{O}_{3+y}$ system

O. F. de Lima,<sup>1,a)</sup> J. A. H. Coaquira,<sup>2</sup> R. L. de Almeida,<sup>3</sup> L. B. de Carvalho,<sup>3</sup> and S. K. Malik<sup>3</sup>

<sup>1</sup>*Instituto de Física Gleb Wataghin, UNICAMP, 13083-970 Campinas, São Paulo, Brazil*

<sup>2</sup>*Núcleo de Física Aplicada, Instituto de Física, UnB, 70904-970 Brasília, Distrito Federal, Brazil*

<sup>3</sup>*Centro Internacional de Física da Matéria Condensada, UnB, 70904-970 Brasília, Distrito Federal, Brazil*

(Received 18 August 2008; accepted 11 November 2008; published online 6 January 2009)

We have investigated the crystal structure and magnetic properties for polycrystalline samples of  $\text{LaMn}_{1-x}\text{Fe}_x\text{O}_{3+y}$ , in the whole range  $0.0 \leq x \leq 1.0$ , prepared by solid state reaction in air. All samples show the ORT-2 orthorhombic structure that suppresses the Jahn–Teller distortion, thus favoring a ferromagnetic (FM) superexchange interaction between  $\text{Mn}^{3+}-\text{O}-\text{Mn}^{3+}$ . For  $x=0.0$  the oxygen excess ( $y \approx 0.09$ ) produces vacancies in the La and Mn sites and generates a fraction around 18% of  $\text{Mn}^{4+}$  ions and 82% of the usual  $\text{Mn}^{3+}$  ions, with possible double-exchange interaction between them. The Fe doping in this system is known to produce only stable  $\text{Fe}^{3+}$  ions. We find an evolution from a fairly strong FM phase with a Curie temperature  $T_C \sim 160$  K, for  $x=0.0$ , to an antiferromagnetic (AFM) phase with  $T_N=790$  K, for  $x=1.0$ , accompanied by clear signatures of a cluster-glass behavior. For intermediate Fe contents a mixed-phase state occurs, with a gradual decrease (increase) in the FM (AFM) phase, accompanied by a systematic transition broadening for  $0.2 < x < 0.7$ . A model based on the expected exchange interaction among the various magnetic-ion types accounts very well for the saturation magnetization ( $M_S$ ) dependence on Fe doping.

© 2009 American Institute of Physics. [DOI: [10.1063/1.3054323](https://doi.org/10.1063/1.3054323)]

### I. INTRODUCTION

The study of manganites started almost 60 years ago,<sup>1,2</sup> with discussions on the occurrence of mixed-valence states and strong ferromagnetic (FM) interaction between the  $\text{Mn}^{3+}$  and  $\text{Mn}^{4+}$  ions, in the  $(\text{La}_{1-x}\text{Ca}_x)\text{MnO}_3$  and  $(\text{La}_{1-x}\text{Sr}_x)\text{MnO}_3$  systems. After the discovery of large magnetoresistance<sup>3</sup> and colossal magnetoresistance (CMR) (Ref. 4) effects in manganite thin films, about 15 years ago, interest on the study of these materials has been revived.

The stoichiometric parent manganite,  $\text{LaMnO}_3$ , is an A-type antiferromagnetic (AFM) insulator, with a Néel temperature ( $T_N$ ) of 140 K. In this compound all Mn ions are trivalent and coupled through a superexchange (SE) interaction<sup>5,6</sup> that produces a FM coupling within the *a-c* planes in its orthorhombic structure, and an AFM coupling between these planes, along the *b* direction (space group *Pnma*). When a fraction of trivalent La ions is substituted by divalent alkaline earth ions (e.g., Sr and Ca) the same fraction of  $\text{Mn}^{3+}$  is transformed to  $\text{Mn}^{4+}$ , and an electron will be allowed to hop between these ions producing a FM double-exchange (DE) interaction,<sup>7</sup> which also promotes a metallic electric conduction.

Much of the work done so far to explore manganite properties<sup>8,9</sup> has been mainly focused on the effects produced by doping the La sites, such as the lattice distortions that ultimately influence the DE and SE interactions. Also playing an important role are the combined effects derived from spin, charge, and orbital degrees of freedom,<sup>10</sup> typical in strongly correlated electron systems. The occurrence of a magnetic mixed-phase state in manganites, consisting of short-range-ordered regions that coexist with long-range-

ordered regions, is by now strongly supported by many experimental<sup>11–14</sup> and theoretical<sup>15,16</sup> results. In that context the various possibilities of charge-, spin-, and orbital-ordered configurations play a central role.

Substitutions on the Mn site by various 3*d* cations (Cr, Co, Ni, and Fe) have been explored<sup>17–25</sup> in the past years, mainly motivated by the fact that Mn is the main actor in the DE interaction, and also to test interesting ideas related to other possible coupling mechanisms between Mn ion and the doping cation. For instance, a FM SE interaction between  $\text{Mn}^{3+}-\text{O}-\text{Mn}^{3+}$  has been proposed and actually verified in the system<sup>26</sup>  $\text{LaMn}_{1-x}\text{B}_x\text{O}_{3+y}$  (*B*=Ga, Co, Ni). There is also the idea of a FM coupling caused by a DE interaction between  $\text{Fe}^{3+}-\text{O}-\text{Mn}^{3+}$  in the  $\text{LaMn}_{1-x}\text{Fe}_x\text{O}_3$  system.<sup>21</sup> In this paper we will be presenting strong evidences for the FM coupling via SE interaction between  $\text{Mn}^{3+}$  ions, for the case of  $\text{LaMn}_{1-x}\text{Fe}_x\text{O}_{3+y}$ . The substitution of  $\text{Fe}^{3+}$  ( $S=5/2$ ) for  $\text{Mn}^{3+}$  ( $S=2$ ) is special, in the sense that both these ions have the same ionic radius<sup>8,27</sup> and different magnetic moments in their high-spin states. This means that in this case lattice distortions can be avoided and any existing magnetic change has a good chance to be appropriately detected.

Until recently all studies of Fe doping Mn sites were done in the usual CMR compounds  $\text{La}(\text{Sr}, \text{Ca})\text{Mn}_{1-x}\text{Fe}_x\text{O}_3$ . Typically they found<sup>19,20</sup> that electric conduction and ferromagnetism were consistently suppressed by Fe doping, and CMR was shifted to lower temperatures being enhanced by Fe doping in some cases. However, doping the simpler parent compound  $\text{LaMnO}_3$  could help to identify the real influence of Fe on the structure. This would avoid more complex effects related to structural and electronic modulations in the La–O layers. With that motivation, recently some few works have produced results on the structural, transport, and magnetic properties of the  $\text{LaMn}_{1-x}\text{Fe}_x\text{O}_{3+y}$  system. In general

<sup>a)</sup>Electronic mail: delima@ifi.unicamp.br.

these studies<sup>21–24</sup> agree with the suppression of ferromagnetism by increasing Fe doping, in reason of the gradual substitution of  $\text{Mn}^{3+}$  by  $\text{Fe}^{3+}$  that reduces the amount of DE-coupled  $\text{Mn}^{4+}-\text{O}-\text{Mn}^{3+}$  bonds. Also they agree on the occurrence of a cluster-glass (CG)-like behavior, with complicated features, mainly for higher Fe doping. However, the only work that covers a broad range of compositions, with  $0.05 \leq x \leq 0.95$ , has reported<sup>25</sup> an increase in the sample magnetic moment with  $x$ , in contradiction with all the other studies. In an attempt to clarify this problem we offer here a comprehensive description of the magnetic phase evolution, for the whole range of Fe doping, in the  $\text{LaMn}_{1-x}\text{Fe}_x\text{O}_{3+y}$  system.

In this paper we present a thorough study of the crystal structure and magnetic properties for a relatively large set of  $\text{LaMn}_{1-x}\text{Fe}_x\text{O}_{3+y}$  samples with  $0.0 \leq x \leq 1.0$ . We found a suppression of ferromagnetism while  $x$  increases, and a complex evolution of a mixed-phase state, with clear signatures for the occurrence of a CG in the whole doping range. A model that describes accurately the saturation magnetization of all samples, based on the evolution of possible magnetic phases, is proposed and discussed.

## II. EXPERIMENTAL DETAILS

A set of nine samples of composition  $\text{LaMn}_{1-x}\text{Fe}_x\text{O}_{3+y}$ , for  $0.0 \leq x \leq 1.0$ , was reacted using the solid diffusion method in open air. For each sample we started with the stoichiometric mixture of  $\text{La}(\text{OH})_3$ ,  $\text{Mn}_2\text{O}_3$ , and  $\text{Fe}_2\text{O}_3$  powders, which was fired in a tubular furnace at the temperature of 1100 °C for 24 h. Following, the prereacted sample was crushed and thoroughly milled with a mortar and pestle, then pressed in a cylindrical die and returned to the furnace for a reaction and sintering treatment, again at 1100 °C for 24 h. After the samples were prepared, small pieces with masses in the range 20–80 mg were cut from them for the magnetic measurements. Also small pieces were pulverized for the x-ray experiments, which were done in a Phillips diffractometer at  $T \approx 300$  K, using  $\text{Cu } K\alpha$  radiation.

It is well established that a perovskite structure cannot accept excess  $\text{O}^{2-}$  ions in an interstitial site.<sup>8</sup> Actually it has been shown that any oxygen excess  $y$  in the nonstoichiometric compound  $\text{LaMnO}_{3+y}$  is accommodated as cation vacancies.<sup>28,29</sup> Therefore, from a crystallographic point of view, a more appropriate formula would be  $\text{La}_{1-z}\text{Mn}_{1-z}\text{O}_3$ , where  $z=y/(3+y)$ , by assuming an equal amount of La and Mn vacancies.<sup>29</sup> In this paper, however, for simplicity, we adopt the formula  $\text{LaMn}_{1-x}\text{Fe}_x\text{O}_{3+y}$ , considering that vacancies are equally distributed in the La and Mn sites.

Figure 1 shows the x-ray spectra for seven samples, covering the whole range of iron doping. All of them, as well as the samples with  $x=0.05$  and  $0.50$  (not shown), produced similar spectra, where the corresponding peaks fall essentially at the same angular positions. However, for  $x > 0.7$ , a slight decrease in the angular distance between peaks is observed, revealing a small increase in the lattice spacing. These results are consistent with the well established fact that iron occupies the manganese sites always in the valence state<sup>21,30</sup>  $\text{Fe}^{3+}$  that has essentially the same ionic radius of

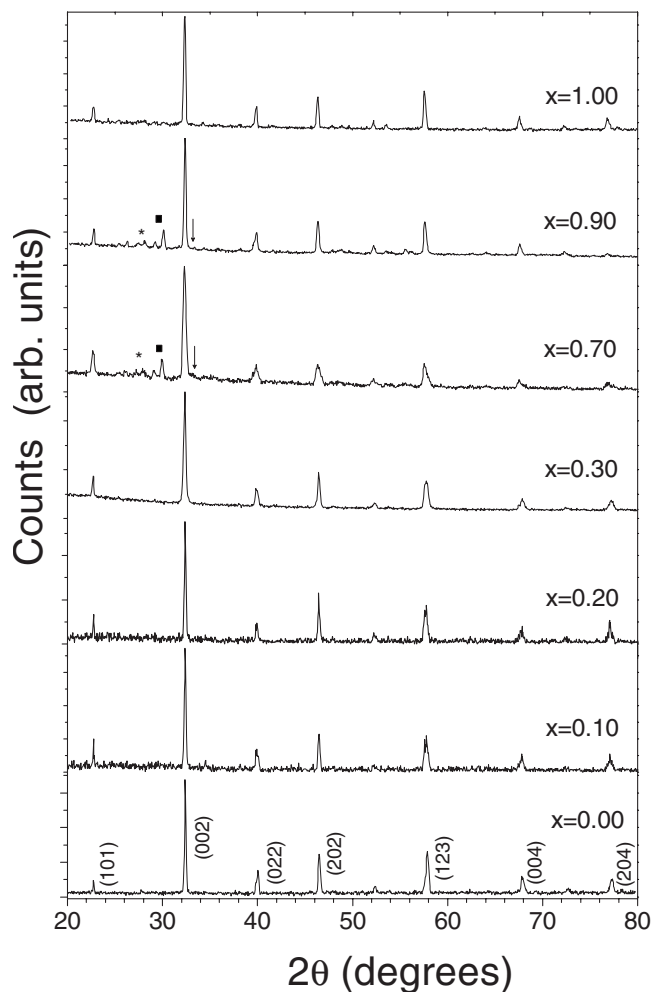


FIG. 1. X-ray diffraction patterns for  $\text{LaMn}_{1-x}\text{Fe}_x\text{O}_{3+y}$  samples, measured with  $\text{Cu } K\alpha$  radiation at  $T \approx 300$  K. The numbers in parentheses near the peaks of sample with  $x=0.0$  are the Miller indices corresponding to the main crystallographic planes. The strongest peaks of impurities are marked with a solid square ( $\text{La}_2\text{O}_3$ ), an asterisk [ $\text{La}(\text{OH})_3$ ], and a down arrow ( $\alpha\text{-Fe}_2\text{O}_3$ ), being detected mainly in samples with  $x \geq 0.5$ .

$\text{Mn}^{3+}$ , whose value is<sup>27</sup> 0.645 Å. On the other hand, the  $\text{Mn}^{4+}$  ionic radius is smaller ( $\sim 0.530$  Å),<sup>27</sup> thus causing some lattice expansion when a  $\text{Mn}^{4+}$  site is occupied by an  $\text{Fe}^{3+}$  ion.

Analysis of all diffraction patterns by the Rietveld method indicated that all samples contain at least 90% of pure manganite phase, with an orthorhombic structure (space group  $Pnma$ ). The main impurities detected for  $x=0.7$  and  $x=0.9$  have their strongest peaks marked in Fig. 1 by a solid square ( $\text{La}_2\text{O}_3$ ), an asterisk [ $\text{La}(\text{OH})_3$ ], and a down arrow ( $\alpha\text{-Fe}_2\text{O}_3$ ). The calculated lattice parameters for the low end composition ( $x=0.0$ ) are  $a=5.535$  Å,  $b=7.786$  Å, and  $c=5.500$  Å, within the expected values that characterize the so-called  $O$ -type orthorhombic structure (ORT-2)<sup>31,32</sup> where  $c < b/2^{1/2} < a$ . This structure suppresses the Jahn–Teller distortion, which involves a cooperative rotation of the  $\text{MnO}_6$  octahedras, and favors an isotropic FM SE interaction<sup>5</sup> between  $\text{Mn}^{3+}-\text{O}-\text{Mn}^{3+}$ . In contrast, the more usual  $O'$ -orthorhombic structure (ORT-1),<sup>5,31–33</sup> where  $b/2^{1/2} < c < a$ , stabilizes the Jahn–Teller distortion and favors a canted-AFM SE interaction between  $\text{Mn}^{3+}-\text{O}-\text{Mn}^{3+}$ . The ORT-1

TABLE I. Magnetic properties of the  $\text{LaMn}_{1-x}\text{Fe}_x\text{O}_{3+y}$  samples, calculated from magnetization measurements taken with a SQUID magnetometer.  $T_C$  and  $\theta_W$  are the Curie and Weiss temperatures, respectively;  $\mu_{\text{eff}}$  is the effective moment in the PM state;  $\mu_{H,2\text{ K}}$  and  $\mu_{H,300\text{ K}}$  are the saturation moments at 2 and 300 K; and  $H_{C,2\text{ K}}$  and  $H_{C,300\text{ K}}$  are the coercivities at 2 and 300 K. The magnetic moments are given in units of  $\mu_B/\text{f.u.}$

$x$	$T_C$ (K)	$\theta_W$ (K)	$\mu_{\text{eff}}$ ( $\mu_B/\text{f.u.}$ )	$\mu_{H,2\text{ K}}$ ( $\mu_B/\text{f.u.}$ )	$\mu_{H,300\text{ K}}$ ( $10^{-2}\mu_B/\text{f.u.}$ )	$H_{C,2\text{ K}}$ (Oe)	$H_{C,300\text{ K}}$ (Oe)
0.00	160(1)	189(2)	5.88(2)	3.75(1)	0.030(3)	35(1)	7(1)
0.05	153(1)	175(2)	5.91(1)	3.30(1)	0.199(3)	26(1)	12(1)
0.10	133(1)	150(2)	6.16(1)	2.96(2)	0.303(3)	87(1)	8(1)
0.20	110(2)	130(2)	5.74(1)	1.94(2)	0.395(4)	425(4)	18(1)
0.30	62(3)	113(2)	4.41(1)	1.02(2)	...	1900(20)	80(2)
0.50	65(3)	111(2)	4.53(3)	0.61(3)	0.520(4)	1160(20)	170(5)
0.70	50(3)	85(3)	3.77(3)	0.25(3)	0.557(4)	1790(20)	470(10)
0.90	43(4)	22(4)	4.02(5)	0.08(3)	0.648(5)	2900(20)	8 000(100)
1.00	65(3)	40(2)	3.10(5)	0.07(2)	1.448(5)	1800(20)	17 500(200)

structure is typically observed for  $\text{LaMnO}_{3+y}$  with  $y < 0.05$ , when reacted in a reducing or oxygen-depleted atmosphere, while samples reacted in air have normally the ORT-2 structure,<sup>8,31,32</sup> with  $y \approx 0.09$ . Since in our work all reactions were processed in air, we then assume an oxygen excess of  $y=0.09$  in all samples, following the typical values reported by different authors.

Table I lists all samples and several of their magnetic properties, extracted from a large number of magnetization curves that were taken with a Quantum Design superconducting quantum interference device (SQUID) magnetometer. Zero field cooled (ZFC) and field cooled (FC) measurements were done in almost all cases. In order to warrant the same initial conditions for the magnet residual field and for the samples' magnetic state, before each ZFC curve a field of 5 kOe was applied and lowered to zero through oscillations at  $T=300\text{ K}$ . Then the temperature was lowered to 2 K, where the measuring field was applied and the measurements were taken during a slow warming ramp, up to 320 K. Following, the FC curve was taken in a cooling ramp, using the same rate, down to 2 K. ac susceptibility measurements were taken with a physical property measurement system from Quantum Design.

### III. RESULTS AND DISCUSSIONS

Typical magnetization curves for all samples, under a reasonably small applied field of 100 Oe, are shown in Fig. 2(a). Clearly there is a ferromagneticlike (FM-like) transition that looks sharp for small iron contents ( $x \leq 0.1$ ). However, this transition becomes broader and is shifted to lower temperatures, showing smaller intensity, for higher  $x$  values. Indeed, one can see in the inset of Fig. 2(a) that even for  $x=1.0$ , the high end composition also exhibits a clear, although weak, FM-like signature. Since  $\text{LaFeO}_3$  is known to present an AFM coupling with spin canting,<sup>34</sup> we believe this is possibly the origin for the observed weak ferromagnetism. Another relevant feature present in the  $M \times T$  curves is the strong irreversibility between the ZFC and FC curves, typical of a superparamagnetic (SPM) relaxation phenomena of a CG system.<sup>35–38</sup> In fact, several features, which will be highlighted along this paper, support the likely occurrence of a CG in our  $\text{LaMn}_{1-x}\text{Fe}_x\text{O}_{3+y}$  samples, similar to the results for

some compositions of this system reported by other authors.<sup>23,39</sup> For instance, all of our ZFC curves show a maximum at a temperature  $T_p$  (around 150 K for  $x=0.0$ ) below the FM-like transition, and a shoulder at a lower tem-

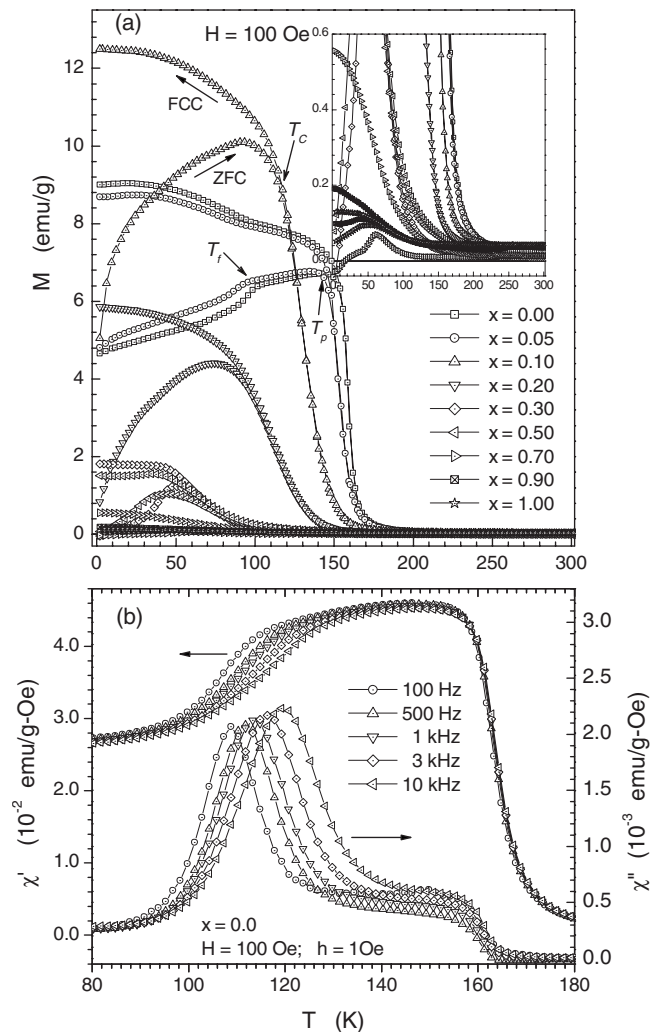


FIG. 2. (a) ZFC and FC magnetization curves of all  $\text{LaMn}_{1-x}\text{Fe}_x\text{O}_{3+y}$  samples, measured with  $H=100\text{ Oe}$ ; (b) real (left axis) and imaginary (right axis) components of magnetic ac susceptibility, measured in the sample with  $x=0.0$ , at different frequencies. The inset of (a) is a magnified view that helps to observe the FM-like transitions for samples with  $x \geq 0.7$ .

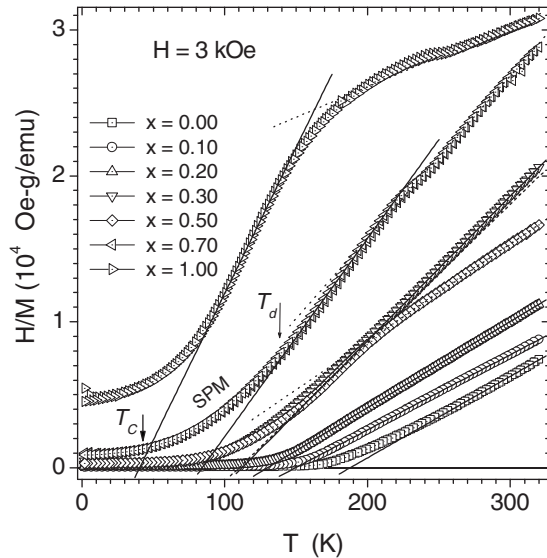


FIG. 3. Plot of the inverse susceptibility  $H/M$  as a function of temperature, measured under  $H=3$  kOe in ZFC and FC modes. A simple Curie-Weiss behavior (solid lines) is seen for  $x \leq 0.2$ , while for  $x \geq 0.3$  the curves bend to the right after a limited interval of straight-line behavior.

perature  $T_f$  (around 100 K for  $x=0.0$ ) that fades out for higher  $x$  values. Figure 2(b) shows some ac susceptibility measurements for sample  $x=0.0$  confirming the occurrence of these especial temperatures, by showing a frequency-dependent (-independent) maximum at  $T_f(T_p)$  in the imaginary components, accompanied by corresponding inflexion points in the real components. Several characteristics of  $T_p$  and  $T_f$ , whose details will be published elsewhere, typify  $T_p$  as an average blocking temperature where the clusters' moments begin to freeze in a field  $H$ , and  $T_f$  as the temperature where this thermally activated freezing process reaches a maximum. Consistent with that picture there is a strong field dependence, revealed by a complete suppression of the magnetic irreversibility down to  $T=2$  K, for relatively small values of  $H$ , as can be seen in Fig. 3 for  $H=3$  kOe. This might be due to a full alignment of the clusters' moments in the magnetic field direction, as already observed in  $\text{LaMnO}_{3+y}$  samples<sup>40</sup> with  $y \leq 0.15$ . Similar observations were also reported for nanoparticles of  $\gamma\text{-Fe}_2\text{O}_3$  incorporated in a resin matrix,<sup>41</sup> as well as for amorphous Pd-Ni-Fe-P alloys.<sup>42</sup>

Figure 4 shows plots of the virgin magnetization curves as a function of  $H/T$ , for the sample with  $x=0.3$ . These curves are spaced from each other by 3 K, in the interval from 26 to 68 K. One sees that five curves for  $T \geq 56$  K superimpose almost perfectly, thus following what is predicted to happen for SPM spin clusters,<sup>43</sup> while for  $T < 56$  K the curves gradually break away. A complementary test is shown in the inset of Fig. 4 where an Arrott plot,<sup>44</sup>  $M^2 \times H/M$ , is performed for the same set of isothermal curves. In this standard experimental method the occurrence of FM order is predicted to occur when straight lines  $M^2 \propto H/M$  are obtained in the plots. Further, it defines the Curie temperature ( $T_C$ ) of the isotherm whose linear extrapolation intercepts the vertical axis at the value zero. In the present case we find  $T_C \approx 56$  K (black dots in Fig. 4) for the sample with  $x=0.3$ , in excellent agreement with the temperature

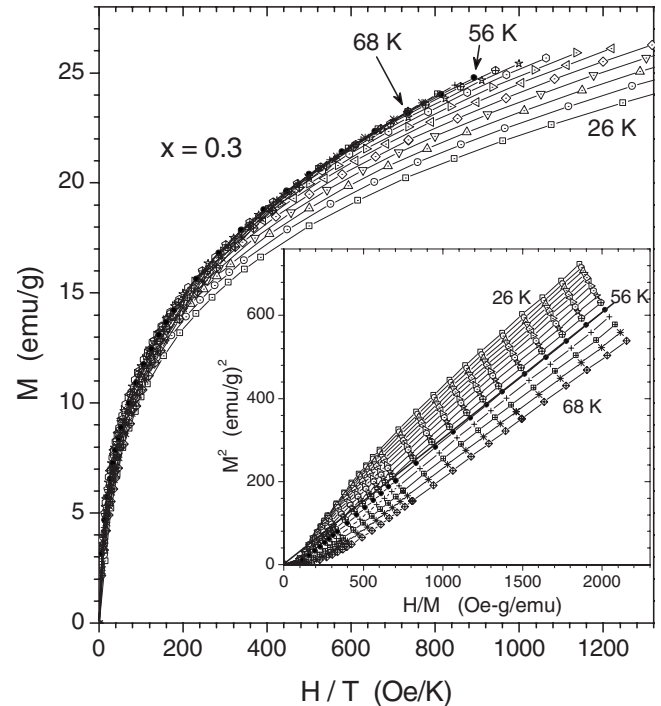


FIG. 4. The main frame shows a scaling plot of the virgin magnetization as a function of  $H/T$ , for a sample with  $x=0.3$ , showing the collapse of five isothermal curves from 56 to 68 K, suggesting a SPM behavior. The inset is an Arrott's plot for the same set of isotherms that varies from 26 to 68 K, in steps of 3 K, revealing a Curie temperature of 56 K.

value that limits the SPM behavior, according to the first test of Fig. 4. We conclude, then, that a SPM regime occurs for  $T > T_C$ , while a FM-like order is established for  $T \leq T_C$ . It is worth noticing that the down curvatures in Arrott's plots, at low fields and especially for the lower temperature isotherms, are usually observed in granular and amorphous ferromagnets.<sup>42,45</sup> The  $T_C$  values listed in Table I were defined at the inflexion point where the derivative  $dM/dT$  has a maximum value [see Fig. 2(a)]. This is a simpler and commonly used criterion, although it furnishes  $T_C$  values that are slightly above those obtained through Arrott plots. In this work the  $T_C$  values coincide with the point where the ZFC and FC curves bifurcate, for samples having  $x \leq 0.2$ . For samples with higher iron contents  $T_C$  is located below the bifurcation point, thus indicating a more complex dynamics of the SPM clusters.

We assume that a short-range order FM-like state is induced by the applied magnetic field, in the region between the SPM and CG states ( $T_f < T < T_C$ ), following the same interpretation applied to similar data obtained with amorphous alloys.<sup>42,46</sup> In our work three facts give support to this hypothesis: (i) the relatively high and positive values of the calculated Weiss constant ( $\theta_w$ ) (Table I), (ii) the Arrott plots typical of FM materials (inset of Fig. 4), and (iii) the clear separation between the SPM and FM-like regimes shown in the scaling plot of Fig. 4. However, it is not clear at the moment what would be the microscopic mechanism that could provide such FM-like order among the SPM clusters.

Figure 3 shows a plot of the inverse susceptibility  $H/M$  as a function of temperature for seven samples, measured under  $H=3$  kOe in ZFC and FC modes. For  $0.0 \leq x \leq 0.2$ , a

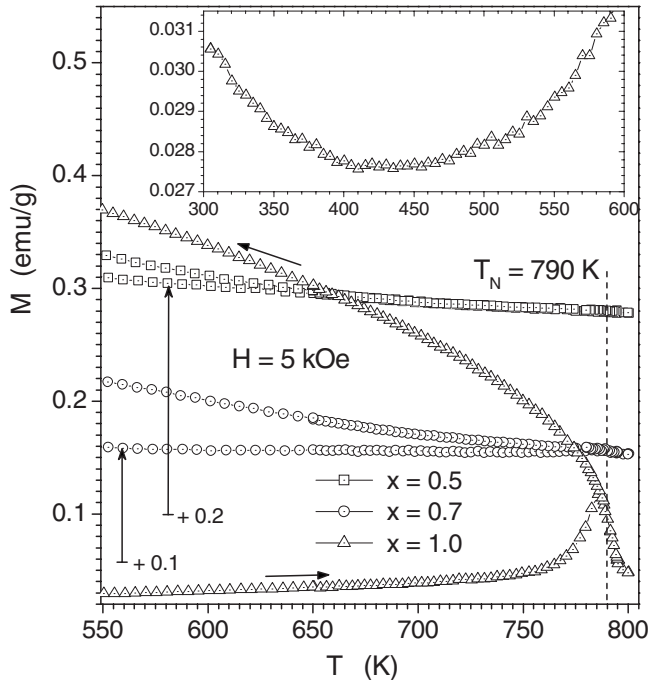


FIG. 5. High-temperature magnetization curves of samples with  $x=0.5, 0.7$ , and  $1.0$ , measured in the range of temperatures between  $300$  and  $800$  K and under  $H=5$  kOe. A clear AFM transition is seen for  $x=1.0$  ( $\text{LaFeO}_{3+y}$ ) at  $T_N \approx 790$  K. The inset is an enlarged view of the ZFC curve for  $\text{LaFeO}_{3+y}$ , showing a monotonical decrease that changes to a monotonical increase around  $430$  K, speeding up very quickly above  $750$  K.

large part of the higher-temperature region follows a linear behavior as predicted for a PM phase according to the Curie–Weiss law,  $M/H=C/(T-\theta_W)$ , where  $C$  and  $\theta_W$  are the Curie and Weiss constants, respectively. Therefore, the slope of a straight line fitted in the linear region (solid lines in Fig. 3) gives  $1/C$  and its intercept with the temperature axis gives  $\theta_W$ . Since the effective magnetic moment per f.u. can be expressed, in Bohr magnetons ( $\mu_B$ ), by<sup>47</sup>  $\mu_{\text{eff}}=(3k_B C A/N_A)^{1/2} \approx 2.829(AC)^{1/2}$ , where  $k_B$  is the Boltzmann constant,  $A$  is the molecular weight, and  $N_A$  is the Avogadro number, one can see from Fig. 3 that  $\mu_{\text{eff}}$  in general decreases when  $x$  increases. But the experimentally determined  $\mu_{\text{eff}} \approx 5.9 \mu_B/\text{f.u.}$  for sample  $x=0$  (Table I) exceeds the spin-only value given by  $g[S(S+1)]^{1/2}$ , with  $g=2$ , even if we assume the overestimated situation of having all manganese ions  $\text{Mn}^{3+}$  in their high-spin state ( $S=2$ ), which would give  $4.9 \mu_B/\text{f.u.}$  for sample  $x=0.0$ . The other extreme with  $x=1.0$  is more complicated, since  $\text{LaFeO}_{3+y}$  is expected to be in a canted-AFM state up to  $T_N$  with no room, in principle, for a PM state when  $T < 790$  K (see Fig. 5). Unless, of course, if an existing cluster system, as already assumed, could explain the transition from a FM-like state to a PM-like state, by increasing the temperature. However, we are not aware of any model that could provide a calculation of  $\mu_{\text{eff}}$  in such a cluster system, for the case of  $x > 0.0$  in our samples.

The well behaved trend, just described above, changes for iron contents  $x \geq 0.3$ , where two regions become gradually evident in Fig. 3 as  $x$  increases. In the first region, right above the curved section between the FM-like to SPM states, is observed a linear behavior (solid lines) that maintains

more or less the same trend as observed in samples with  $x \leq 0.2$ , where  $\mu_{\text{eff}}$  and  $\theta_W$  decrease gradually while  $x$  increases. Concomitantly, the second region bends to the right and departs progressively from the initial linear behavior (dashed lines). Other studies,<sup>30,48</sup> on the single composition  $\text{LaMn}_{0.5}\text{Fe}_{0.5}\text{O}_3$ , also revealed this intriguing curvature in their  $H/M$  data, whose origin was attributed to the occurrence of magnetic clusters. We agree with that interpretation and, indeed, our data support a broader and more complete description of this phenomenon, based on the global magnetic evolution manifested by the whole set of samples ( $0.0 \leq x \leq 1.0$ ).

The temperature  $T_d$ , indicated in the curve for  $x=0.7$  (Fig. 3), has been identified<sup>42</sup> as a transition point that separates a linear PM region, corresponding to the usual single magnetic moment per f.u., from a curved SPM region, where the number of aligned moments gradually increases inside the clusters down to  $T_C$ . We partially agree with that interpretation, the only difference being that in our case a situation with a single moment per f.u. was not observed, although a PM-like Curie–Weiss description seems to work well.

In an attempt to shed more light on the problem, we now discuss the  $M \times T$  curves of samples with  $x=0.5, 0.7$ , and  $1.0$  (Fig. 5), taken in the range of temperatures between  $300$  and  $800$  K and under a magnetic field of  $5$  kOe. A clear AFM transition occurs for the end compound  $\text{LaFeO}_{3+y}$  at  $T_N \approx 790$  K, which is larger than the value of  $740$  K found in Mössbauer studies.<sup>34</sup> The strong irreversibility between the ZFC and FC curves, again, indicates the occurrence of a CG system, plausibly formed by weak-FM domains or clusters of the canted-AFM phase.<sup>34</sup> For the samples  $x=0.5$  and  $0.7$  the ordering transition around  $790$  K is not convincingly resolved, possibly due to a combination of two factors, the smaller relative content of the  $\text{LaFeO}_{3+y}$  compound and a limited sensitivity of the measuring technique. However, it is very interesting to observe the gradual increase in irreversibility, consistent with the progressive formation of  $\text{LaFeO}_{3+y}$  as  $x$  increases. Notice also that these  $M \times T$  curves are shifted vertically by  $0.2$  and  $0.1$  emu/g, as indicated by the vertical arrows in Fig. 5, aimed at solely to improve the clarity of presentation.

The inset in the upper part of Fig. 5 displays an enlarged view of the ZFC curve for  $\text{LaFeO}_{3+y}$ . In fact, it matches very nicely with the end of the ZFC magnetization curve measured between  $2$  and  $320$  K (not shown). However, the monotonical decrease in  $M(T)$  that starts above  $T_C=65$  K [see inset of Fig. 2(a)] is smoothly changed to a monotonical increase around  $430$  K, speeding up very quickly above  $750$  K. Without discussing the details of the underlying CG dynamics, we can conclude that this result must certainly affect the Curie–Weiss behavior observed in the first region of Fig. 3 (solid lines). Therefore, we believe this could be the origin of the unusual bending to the right, observed in the second region of Fig. 3 (dashed lines). This would account naturally for the gradually larger curvatures occurring for higher  $x$  values, which could be ascribed simply to the stronger presence of  $\text{LaFeO}_{3+y}$ . In other words, one could think that right above the first region starts a convoluted regime that com-

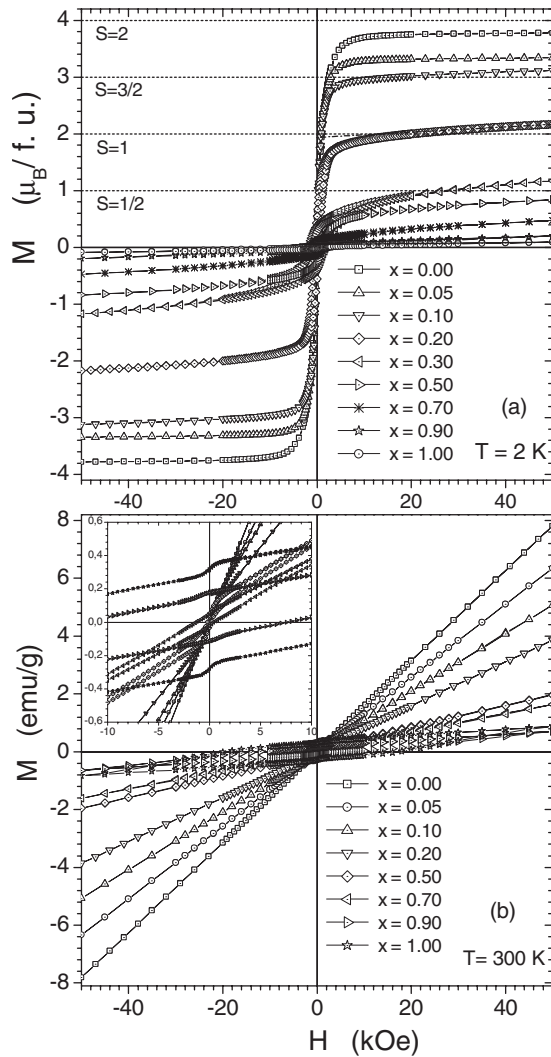


FIG. 6. Magnetization as a function of field for all samples, measured at 2 (a) and 300 K (b). Magnetization is expressed in  $\mu_B/f.u.$  in (a), and  $S$  values indicate the high-spin states. For samples with  $x \geq 0.2$ , hysteresis gradually increases with  $x$  in both temperatures. The inset in (b) magnifies a region near the origin, making clear the manifestation of high coercivities for  $x \geq 0.9$ .

binates the Curie–Weiss behavior, connected with the SPM region at low temperature, with some other functional dependence that accounts for the high-temperature behavior of  $\text{LaFeO}_{3+y}$ .

Magnetization curves of complete  $M \times H$  loops were measured for all samples, starting at  $H=0$  and then cycling between 50 and  $-50$  kOe, at the temperatures of 2 [Fig. 6(a)] and 300 K [Fig. 6(b)]. The curves for samples with  $x \leq 0.1$  are almost reversible presenting very small coercivities,  $H_{C,300\text{ K}} < 10$  Oe at 300 K and  $H_{C,2\text{ K}} < 100$  Oe at 2 K (see Table I and Fig. 7), common in systems of almost noninteracting SPM clusters or particles. However, for  $x \geq 0.2$ , a visible hysteresis appears at low fields and coercivity gradually increases. Curiously for  $x \geq 0.7$  coercivity values seem to stay around 2 kOe when measured at 2 K, in contrast with a steep increase that reaches 17.5 kOe for sample  $x=1.0$ , when measured at 300 K.

The saturation magnetization at 2 K ( $\mu_{H,2\text{ K}}$ ) was determined at the ordinate point intercepted by the linear extrap-

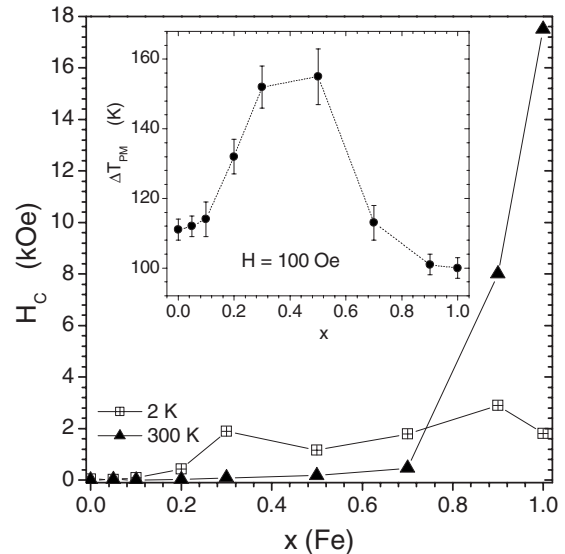


FIG. 7. Coercivity as a function of iron doping  $x$ , calculated from  $M \times H$  curves taken at 2 and 300 K. The inset shows a plot of  $\Delta T_{\text{SPM}} = T_d - T_C$ , which is the temperature width of the main SPM region (see Fig. 3) as a function of  $x$ , evaluated from measurements taken with  $H=100$  Oe.

lation from the straight high-field region of  $M \times H$ . This criterion eliminates the linear nonsaturating behavior, which is increasingly visible for samples with  $x \geq 0.2$ , due probably to the growing presence of canted-AFM clusters of  $\text{LaFeO}_{3+y}$ . Consistent with that hypothesis, one sees in Fig. 6(a) that  $\mu_{H,2\text{ K}}$  can definitely attain its saturated values for magnetic fields around 30 kOe, when  $x \leq 0.1$ .

The canting angle for AFM ordered  $\text{LaFeO}_3$  was determined through Mössbauer studies<sup>34</sup> to be  $\alpha = \mu_{\text{FM}}/2\mu_{\text{Fe}} \approx 0.009$  rad, where  $\mu_{\text{FM}}$  is the measured canted FM component and  $\mu_{\text{Fe}}$  is the  $\text{Fe}^{3+}$  sublattice moment, assumed to be  $5\mu_B$  ( $S=5/2$ ). This  $\alpha$  value was also verified to be practically constant in a broad temperature interval, from  $T_N = 740$  K down to the lowest measured  $T \approx 70$  K. The measured value<sup>34</sup>  $\mu_{\text{FM}} \approx 0.09\mu_B$  is in remarkable agreement with  $\mu_{H,2\text{ K}} \approx 0.07\mu_B$  that was measured in our  $x=1.0$  ( $\text{LaFeO}_{3+y}$ ) sample, as indicated in Table I.

We also calculated the saturation magnetization at 300 K ( $\mu_{H,300\text{ K}}$ ), using the same procedure employed at 2 K, and their values (Table I) are about two orders of magnitude smaller than the  $\mu_{H,2\text{ K}}$  values. The inset of Fig. 6(b) is a magnified view near  $H=0$  that shows an increasing hysteretic behavior for  $x \geq 0.2$ . Since at 300 K only the  $\text{LaFeO}_{3+y}$  clusters must present magnetic order in the sample (neglecting any small amounts of magnetic impurities), we indeed expect that  $\mu_{H,300\text{ K}}$  should increase with  $x$  as found. Interestingly its maximum value of  $0.014\mu_B$ , for  $x=1.0$ , is only about 20% of the fully aligned canted-spin moments of  $\text{LaFeO}_{3+y}$  measured at 2 K. This is probably due to the temperature induced disorder of the canted-AFM clusters, since the canting angle itself is known to be temperature independent<sup>34</sup> in  $\text{LaFeO}_3$ .

The high coercivity values found in our  $x=1.0$  sample is very common in orthoferrites,<sup>47</sup> where typical crystal anisotropies ( $K_a$ ) of the order of  $10^4$  erg/cm<sup>3</sup> are combined with very small saturation magnetization values, usually

smaller than  $8 \text{ emu/cm}^3$ . High coercivity values in  $M \times H$  curves similar to ours were found<sup>49</sup> in bulk polycrystalline (8.4 kOe) and amorphous (11.9 kOe)  $\text{Mn}_3\text{O}_4$ , which is a canted ferrimagnet below  $T_C \approx 42 \text{ K}$ . It is worthwhile to notice that a coercivity value of 1170 Oe has also been reported<sup>30</sup> for a sample of  $\text{LaMn}_{0.5}\text{Fe}_{0.5}\text{O}_3$  at 12 K, close to the value of 1160(10) Oe measured in our sample with  $x = 0.5$ , at 2 K (see Table I). Attributing the origin of coercivity only to crystal anisotropy, we can estimate from our data  $K_d = (\mu_{H,2 \text{ K}})H_{C,2 \text{ K}}/2 \approx 7 \times 10^2 \text{ erg/cm}^3$  at 2 K and  $K_d = (\mu_{H,300 \text{ K}})H_{C,300 \text{ K}}/2 \approx 1.5 \times 10^3 \text{ erg/cm}^3$  at 300 K. The smaller value found at 2 K suggests another origin of coercivity. For instance, it could be that intercluster rotation dominates at low temperatures, while intracluster spin inversion dominates at high temperatures.

The inset of Fig. 7 shows a plot of the transition width,  $\Delta T_{\text{SPM}} = T_d - T_C$ , corresponding to the temperature width of the main SPM region (see Fig. 3) as a function of  $x$ , evaluated from measurements taken under  $H = 100 \text{ Oe}$ . It is reasonable to expect that a distribution of cluster sizes in this region, which evolves from smaller to larger sizes<sup>13,42</sup> when decreasing  $T$ , might affect the magnetic transition width from a PM-like region ( $T > T_d$ ) to a FM-like region ( $T < T_C$ ). Very interestingly the end compositions,  $x \leq 0.1$  and  $x \geq 0.9$ , show relatively narrower transitions when compared to the central region,  $0.2 \leq x \leq 0.7$ . This is a reliable result, even taking in consideration the large error bars of up to  $\pm 16 \text{ K}$  involved in these calculations. A natural explanation for this behavior might be the occurrence of a magnetic mixed-phase region in the intermediate compositions, discussed in more detail in Sec. IV, while near the end compositions it seems that a more uniform cluster size distribution is present.

#### IV. THE MAGNETIC MIXED-PHASE MODEL

Figure 8 shows graphically most of the parameters listed in Table I, which characterize the samples' magnetic behavior. The effective magnetic moment ( $\mu_{\text{eff}}$ ) and saturation moments ( $\mu_{H,2 \text{ K}}$  and  $\mu_{H,300 \text{ K}}$ ) refer to the right ordinate axis in units of  $\mu_B/\text{f.u.}$ , while the Curie ( $T_C$ ) and Weiss ( $\theta_W$ ) temperatures refer to the left axis. Notice that the evaluated error bars more or less coincide or are smaller than the symbols' size in all cases.  $\mu_{\text{eff}}$  starts with a value close to  $5.9\mu_B$  at  $x = 0.0$ , which is higher than the overestimated theoretical value of  $4.9\mu_B$  expected for a spin-only contribution of  $\text{Mn}^{3+}$  ions. As  $x$  increases,  $\mu_{\text{eff}}$  goes down following an oscillating path and reaching a value of  $3.1 \mu_B/\text{f.u.}$  at  $x = 1.0$ , too high for  $\text{LaFeO}_{3+y}$  in its canted-AFM state.<sup>34</sup> All these features possibly happen due to the presence of SPM clusters, as already discussed.  $T_C$  and  $\theta_W$  also go down while  $x$  increases, with  $\theta_W > T_C$  up to  $x = 0.7$ , characteristic of a FM coupling. For  $x \geq 0.9$  there is an inversion,  $T_C > \theta_W$ , that can be attributed<sup>5</sup> to the dominance of AFM interactions.

The saturation magnetization measured at 2 K ( $\mu_{H,2 \text{ K}}$ ) displays a linear decrease, varying from  $3.75(\pm 0.01)\mu_B$  to  $1.02(\pm 0.02)\mu_B$ , when  $x$  goes from 0.0 to 0.30. Then, it suddenly changes the decreasing rate for  $x > 0.30$ , still showing roughly a linear behavior up to  $x = 1.0$ . Following, we present a simple model, based on the magnetic ion evolution ex-

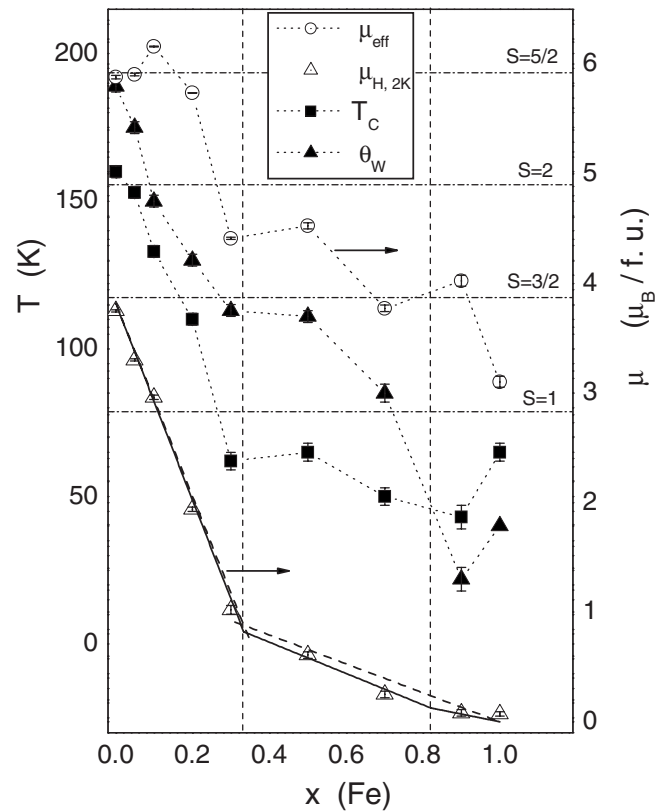


FIG. 8. Most of the magnetic properties listed in Table I are plotted as a function of iron doping  $x$ . The effective magnetic moment ( $\mu_{\text{eff}}$ ) and saturation moments ( $\mu_{H,2 \text{ K}}$  and  $\mu_{H,300 \text{ K}}$ ) refer to the right ordinates in units of  $\mu_B/\text{f.u.}$ , while the Curie ( $T_C$ ) and Weiss ( $\theta_W$ ) temperatures refer to the left ordinates. The vertical dashed lines mark the special concentrations  $x = 1/3$  and  $x = 0.82$ . The horizontal dashed-dotted lines indicate special spin-only values of  $\mu_{\text{eff}}$  given by  $2[S(S+1)]^{1/2}$ .

pected for the whole range of Fe doping, which can provide an excellent description for the  $\mu_{H,2 \text{ K}}$  behavior. A basic general assumption of this model is that iron atoms are incorporated into the  $\text{LaMn}_{1-x}\text{Fe}_x\text{O}_{3+y}$  samples in the form of  $\text{Fe}^{3+}$  ions,<sup>19,30</sup> whose amount grows linearly up to 100%, by occupying the  $\text{Mn}^{3+}$  and  $\text{Mn}^{4+}$  ion sites.

The solid lines in Fig. 9 show in more detail that the initial concentration of 18% for  $\text{Mn}^{4+}$  is assumed to be invariant up to  $x = 0.82$ , where the total amount (82%) of  $\text{Mn}^{3+}$  sites becomes fully occupied. Above that concentration the  $\text{Mn}^{4+}$  sites are then steadily occupied by the  $\text{Fe}^{3+}$  ions up to  $x = 1.0$ . This assumption is motivated by the fact that  $\text{Mn}^{3+}$  ions have the same size<sup>8</sup> ( $0.645 \text{ \AA}$ ) of  $\text{Fe}^{3+}$  ions, while the  $\text{Mn}^{4+}$  ions are smaller ( $0.530 \text{ \AA}$ ), thus requiring a higher activation energy to be replaced with the  $\text{Fe}^{3+}$  ions. The saturation magnetization ( $M_S$ ), represented by the solid lines running very near to the  $\mu_{H,2 \text{ K}}$  points in Fig. 8, was calculated by the following equations, in units of  $\mu_B/\text{f.u.}$ ,

$$M_S = 4(0.82 - x) + 3(0.18) - 5x \quad \text{for } 0 \leq x \leq 1/3, \quad (1)$$

$$M_S = 4(0.82 - x) + (1.28 - 2.22x) + (4.79x - 3.26) \quad \text{for } 1/3 \leq x \leq 0.82, \quad (2)$$

$$M_S = 3(x - 1) + 3.7(1 - x) \quad \text{for } 0.82 \leq x \leq 1.0. \quad (3)$$

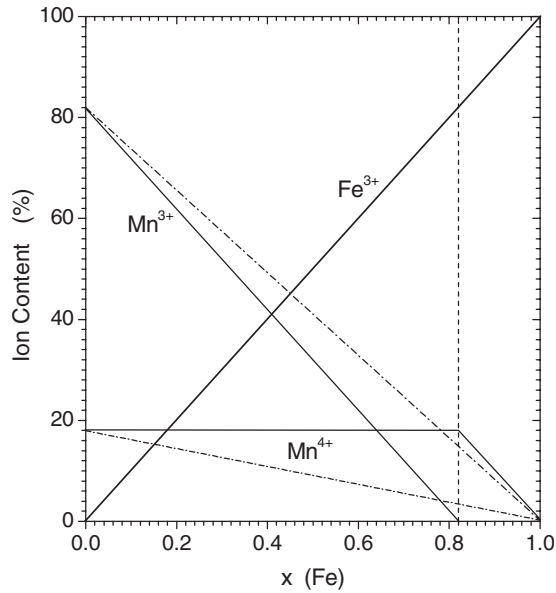


FIG. 9. Mixed-phase model of the ion concentration evolution in the system  $\text{LaMn}_{1-x}\text{Fe}_x\text{O}_{3+y}$ , as a function of iron doping  $x$ .  $\text{Fe}^{3+}$ ,  $\text{Mn}^{3+}$ , and  $\text{Mn}^{4+}$  are assumed to be the only magnetic ions available in the system. The solid lines refer to a more accurate model, while the dashed-dotted lines refer to a simpler and less accurate model.

These equations consider the saturation moment aligned with the magnetic field  $H$  to be  $4\mu_B$  for  $\text{Mn}^{3+}$  ( $S=2$ ),  $3\mu_B$  for  $\text{Mn}^{4+}$  ( $S=3/2$ ), and  $5\mu_B$  for  $\text{Fe}^{3+}$  ( $S=5/2$ ), with all these ions in their high-spin states. The first region is dominated by FM couplings and goes from  $x=0.0$  up to the special concentration  $x=1/3$ . This value is identified as the limit for the higher rate of FM coupling suppression of both types,  $\text{Mn}^{3+}-\text{O}-\text{Mn}^{4+}$  or  $\text{Mn}^{3+}-\text{O}-\text{Mn}^{3+}$ . Up to this concentration, each  $\text{Fe}^{3+}$  makes an AFM coupling with a neighbor  $\text{Mn}^{3+}$  or  $\text{Mn}^{4+}$  and contributes with a magnetic moment of  $5\mu_B$  opposite to the  $H$  direction, as expressed in Eq. (1). It is interesting to notice that all parameters plotted in Fig. 8 suffer an abrupt change at  $x \approx 1/3$ , presenting slower variations above that point, consistent with the increasing dominance of the AFM order. The last region ( $0.82 \leq x \leq 1.0$ ) is simple to analyze, since it admits only AFM couplings of two types,  $\text{Fe}^{3+}-\text{O}-\text{Fe}^{3+}$  or  $\text{Fe}^{3+}-\text{O}-\text{Mn}^{4+}$ . This latter type most possibly allows the spins to flip over, in order to save magnetic energy, by aligning the larger moment of the  $\text{Fe}^{3+}$  ions parallel to  $H$ . Therefore, the term  $3(x-1)$  in Eq. (3) describes a linear suppression of the antiparallel moment for the full content (18%) of  $\text{Mn}^{4+}$ , going from  $-0.54 \mu_B/\text{f.u.}$  to zero. Concomitantly the net moment for a corresponding fraction of 18%  $\text{Fe}^{3+}$  varies from  $3.7 \mu_B/\text{f.u.}$  to zero, as described by the second term of Eq. (3). Here we must notice that this effective moment, smaller than the full value of  $5 \mu_B/\text{f.u.}$  for  $\text{Fe}^{3+}$ , was obtained from a fit to the  $\mu_{H,2 \text{ K}}$  data. Finally, the region  $1/3 \leq x \leq 0.82$  is perhaps the more complex, showing at the same time a decrease in FM and increase in AFM couplings, with the occurrence of spin flips in the latter. By increasing  $x$  the average rate of FM suppression falls with respect to the first region, because part of the  $\text{Fe}^{3+}$  ions will be occupying  $\text{Mn}^{3+}$  sites that already belonged to some pre-existing AFM coupling of the type  $\text{Mn}^{3+}-\text{O}-\text{Fe}^{3+}$ , thus

becoming  $\text{Fe}^{3+}-\text{O}-\text{Fe}^{3+}$ , which is still AFM but with a null contribution to the total magnetic moment. The last term in parentheses of Eq. (2) describes the evolution for the  $\text{Fe}^{3+}$  contribution to the total magnetic moment, by assuming that its effective moment is  $4.79 \mu_B/\text{f.u.}$  in the whole region. This value was found by requiring that the total  $\text{Fe}^{3+}$  moment must be equal to the border values,  $-5/3 \mu_B/\text{f.u.}$  at  $x=1/3$  and  $2/3 \mu_B/\text{f.u.}$  at  $x=0.82$ . This simple phenomenological approach considers that, by connecting linearly the intermediate region with the two well established contiguous regions, a proper account for the combined FM suppression and spin flips in the newly formed AFM bonds becomes guaranteed. Still in the same approach, the middle term in parentheses of Eq. (2) accounts solely for the gradual spin flip of the invariant amount of  $\text{Mn}^{4+}$  ions, whose total magnetic moment goes from  $0.54 \mu_B/\text{f.u.}$  (at  $x=1/3$ ) to  $-0.54 \mu_B/\text{f.u.}$  (at  $x=0.82$ ). The first terms in both Eqs. (1) and (2) describe the linear decrease in the  $\text{Mn}^{3+}$  contribution to the FM couplings in the first region, and to the FM as well as AFM couplings in the second region.

Figure 9 also sketches another possible model, where the  $\text{Mn}^{3+}$  and  $\text{Mn}^{4+}$  ions' evolutions are represented by dashed-dotted lines. Following a similar approach employed in the previous more accurate model the saturation magnetization was calculated and the result is represented by the dashed lines in Fig. 8. Clearly the agreement with the  $\mu_{H,2 \text{ K}}$  data is not good for  $x \geq 1/3$ , although the general trend is maintained. In particular, the small slope change in the data around  $x=0.82$  could not be captured, since this simplistic model assumes a linear decrease in the manganese ions' ( $\text{Mn}^{3+}$  and  $\text{Mn}^{4+}$ ) content in the whole range  $0.0 \leq x \leq 1.0$ .

Finally it is worth mentioning that both models predict  $M_S=0$  for  $x=1.0$ , while the experimental result is  $\mu_{H,2 \text{ K}} = 0.07(2) \mu_B/\text{f.u.}$  This happens because the models do not take into account the very small intrinsic contribution coming from the canted-AFM component of  $\text{LaFeO}_{3+y}$ , as well as eventual contributions arising from possible traces of magnetic impurities.

## V. CONCLUSIONS

We prepared a set of nine samples of polycrystalline  $\text{LaMn}_{1-x}\text{Fe}_x\text{O}_{3+y}$ , with iron doping uniformly distributed in the whole range  $0.0 \leq x \leq 1.0$ , using a solid diffusion reaction method. X-ray diffraction data and Rietveld analysis indicated good quality of samples containing at least 90% of the manganite phase, all of them having an orthorhombic structure (space group  $Pnma$ ). Since the samples were reacted in air we estimated an oxygen excess of  $y=0.09$  in all samples, and the occurrence of the ORT-2 type of orthorhombic structure, where  $c < b/2^{1/2} < a$ , with lattice parameters  $a = 5.535 \text{ \AA}$ ,  $b = 7.786 \text{ \AA}$ , and  $c = 5.500 \text{ \AA}$ , for the sample with  $x=0.0$ .

Magnetization and ac susceptibility measurements allowed a thorough characterization of the magnetic properties at low (2–320 K) and high temperatures (300–800 K). In general, the Curie and Weiss temperatures ( $T_C$  and  $\theta_W$ ), as well as the effective moment ( $\mu_{\text{eff}}$ ) and the saturation moments at 2 and 300 K ( $\mu_{H,2 \text{ K}}$  and  $\mu_{H,300 \text{ K}}$ ), decrease, while

iron doping ( $x$ ) increases. This was interpreted as an evolution of the magnetic phases that starts in  $x=0.0$  with a FM behavior, due to  $\text{Mn}^{3+}-\text{O}-\text{Mn}^{4+}$  DE and  $\text{Mn}^{3+}-\text{O}-\text{Mn}^{3+}$  SE couplings, and evolves to a FM-like behavior, mainly caused by a canted-antiferromagnetism originated from a gradual increase in  $\text{Fe}^{3+}-\text{O}-\text{Fe}^{3+}$  bonds. These bonds belong to the orthoferrite  $\text{LaFeO}_{3+y}$ , the end composition at  $x=1.0$ , that shows a Néel temperature ( $T_N$ ) of 790 K. It is worth noticing that very high coercivities ( $H_C \sim 18$  kOe), typical of orthoferrites, were indeed obtained for  $x=1.0$ .

All samples showed a clear CG behavior, revealed by several features such as the occurrence of irreversible  $M \times T$  curves consistent with the frequency-dependent peak positions in ac susceptibility curves, and a strong field dependence of these irreversibilities, possibly due to the alignment of the cluster's magnetic moments. Several results also suggest the occurrence of a SPM behavior in all samples, such as the excellent overlapping of virgin magnetization curves for temperatures above  $T_C$ , when plotted against the scaling variable  $H/T$ , and  $\mu_{\text{eff}}$  values much larger than the theoretical spin-only predictions. This is especially evident in the high iron doping region ( $x \geq 0.7$ ) where only a small magnetic moment would be expected from a canted-AFM  $\text{LaFeO}_{3+y}$ . Following previous works, we hypothesize that a short-range order (FM-like state) could eventually be induced by the applied magnetic field, in the region between the SPM and CG states.

A magnetic mixed-phase model was proposed, by starting with a basic general assumption that iron atoms are incorporated into the  $\text{LaMn}_{1-x}\text{Fe}_x\text{O}_{3+y}$  structure in the form of  $\text{Fe}^{3+}$  ions, whose amount grows linearly up to 100%, by occupying the  $\text{Mn}^{3+}$  and  $\text{Mn}^{4+}$  ion sites. The estimated initial concentration of 18% for  $\text{Mn}^{4+}$  ( $x=0.0$ ) was assumed to be invariant up to  $x=0.82$ , when the total amount (82%) of  $\text{Mn}^{3+}$  sites becomes fully occupied. Above that concentration the  $\text{Mn}^{4+}$  sites are then steadily occupied by the  $\text{Fe}^{3+}$  ions up to  $x=1.0$ . By considering that all ions are in their high-spin states,  $\text{Mn}^{3+}$  ( $S=2$ ),  $\text{Mn}^{4+}$  ( $S=3/2$ ), and  $\text{Fe}^{3+}$  ( $S=5/2$ ), the model allowed an accurate description of the  $\mu_{H,2\text{K}}$  data in the whole range of iron doping. We expect that the same basic physics involved in this model might apply to any other manganite system, where a similar analysis can be done by taking into account the contributions from the existing magnetic ions.

## ACKNOWLEDGMENTS

We acknowledge the financial support from the Brazilian science agencies Fundação de Amparo à Pesquisa do Estado de São Paulo (FAPESP), Conselho Nacional de Desenvolvimento Científico e Tecnológico (CNPq), and Coordenação de Aperfeiçoamento de Pessoal de Nível Superior (CAPES). One of us (J.A.H.C.) wants to acknowledge also Fundação de Empreendimentos Científicos e Tecnológicos (FINATEC). We also thank Professor A. Ferraz and Professor S. Quezado for the interest in this work.

<sup>1</sup>G. H. Jonker and J. H. van Santen, *Physica (Amsterdam)* **16**, 337 (1950);

J. H. van Santen and G. H. Jonker, *ibid.* **16**, 599 (1950).

<sup>2</sup>G. H. Jonker, *Physica (Amsterdam)* **20**, 1118 (1954).

- <sup>3</sup>R. von Helmolt, J. Wecker, B. Holzapfel, L. Schultz, and K. Samwer, *Phys. Rev. Lett.* **71**, 2331 (1993); K. Chahara, T. Ohno, M. Kasai, and Y. Kozono, *Appl. Phys. Lett.* **63**, 1990 (1993).
- <sup>4</sup>S. Jin, T. H. Tiefel, M. McCormack, R. A. Fastnacht, R. Ramesh, and L. H. Chen, *Science* **264**, 413 (1994).
- <sup>5</sup>J. Töpfer and J. B. Goodenough, *J. Solid State Chem.* **130**, 117 (1997).
- <sup>6</sup>R. Maezono, S. Ishihara, and N. Nagaosa, *Phys. Rev. B* **57**, R13993 (1998).
- <sup>7</sup>C. Zener, *Phys. Rev.* **82**, 403 (1951).
- <sup>8</sup>J. M. D. Coey, M. Viret, and S. von Molnár, *Adv. Phys.* **48**, 167 (1999).
- <sup>9</sup>M. B. Salamon and M. Jaime, *Rev. Mod. Phys.* **73**, 583 (2001).
- <sup>10</sup>J. López, O. F. de Lima, P. N. Lisboa-Filho, and F. M. Araujo-Moreira, *Phys. Rev. B* **66**, 214402 (2002).
- <sup>11</sup>M. Cheong, S. Mori, C. H. Chen, and S.-W. Cheong, *Nature (London)* **399**, 560 (1999).
- <sup>12</sup>T. Becker, C. Streng, Y. Luo, V. Moshnyaga, B. Damaschke, N. Shannon, and K. Samwer, *Phys. Rev. Lett.* **89**, 237203 (2002).
- <sup>13</sup>Y. Murakami, J. H. Yoo, D. Shindo, T. Atou, and M. Kikuchi, *Nature (London)* **423**, 965 (2003).
- <sup>14</sup>N. Veglio, F. J. Bermejo, J. Gutierrez, J. M. Barandiarán, A. Pena, M. A. González, P. P. Romano, and C. Mondelli, *Phys. Rev. B* **71**, 212402 (2005).
- <sup>15</sup>A. Moreo, S. Yunoki, and E. Dagotto, *Science* **283**, 2034 (1999).
- <sup>16</sup>E. Dagotto, *New J. Phys.* **7**, 67 (2005).
- <sup>17</sup>A. Barnabé, A. Maignan, M. Hervieu, and B. Raveau, *Eur. Phys. J. B* **1**, 145 (1998).
- <sup>18</sup>R. Mahendiran, B. Raveau, M. Hervieu, C. Michel, and A. Maignan, *Phys. Rev. B* **64**, 064424 (2001).
- <sup>19</sup>K. H. Ahn, X. W. Wu, K. Liu, and C. L. Chien, *Phys. Rev. B* **54**, 15299 (1996).
- <sup>20</sup>M. M. Xavier, Jr., F. A. O. Cabral, J. H. de Araújo, C. Chesman, and T. Dumelow, *Phys. Rev. B* **63**, 012408 (2000).
- <sup>21</sup>W. Tong, B. Zhang, S. Tan, and Y. Zhang, *Phys. Rev. B* **70**, 014422 (2004).
- <sup>22</sup>K. De, R. Ray, R. N. Panda, S. Giri, H. Nakamura, and T. Kohara, *J. Magn. Magn. Mater.* **288**, 339 (2005).
- <sup>23</sup>K. De, M. Patra, S. Majumdar, and S. Giri, *J. Phys. D* **40**, 7614 (2007).
- <sup>24</sup>D. V. Karpinsky, I. O. Troyanchuk, and V. V. Sikolenko, *J. Phys.: Condens. Matter* **19**, 036220 (2007).
- <sup>25</sup>X.-D. Zhou, L. R. Pederson, Q. Cai, J. Yang, B. J. Scarfino, M. Kim, W. B. Yelon, W. J. James, H. U. Anderson, and C. Wang, *J. Appl. Phys.* **99**, 08M918 (2006).
- <sup>26</sup>J. B. Goodenough, A. Wold, R. J. Armit, and N. Menyuk, *Phys. Rev.* **124**, 373 (1961).
- <sup>27</sup>R. D. Shannon, *Acta Crystallogr., Sect. A: Cryst. Phys., Diff., Theor. Gen. Crystallogr.* **32**, 751 (1976).
- <sup>28</sup>J. H. Kuo, H. U. Anderson, and D. M. Sparlin, *J. Solid State Chem.* **83**, 52 (1989).
- <sup>29</sup>J. A. M. van Roosmalen, E. H. P. Cordfunke, R. B. Helmholtz, and H. W. Zandbergen, *J. Solid State Chem.* **110**, 100 (1994).
- <sup>30</sup>S. D. Bhamé, V. L. Joseph Joly, and P. A. Joy, *Phys. Rev. B* **72**, 054426 (2005).
- <sup>31</sup>B. Hauback, H. Fjellvag, and N. Sakai, *J. Solid State Chem.* **124**, 43 (1996).
- <sup>32</sup>Q. Huang, A. Santoro, J. W. Lynn, R. W. Erwin, J. A. Borchers, J. L. Peng, and R. L. Greene, *Phys. Rev. B* **55**, 14987 (1997).
- <sup>33</sup>C. Ritter, M. R. Ibarra, J. M. de Teresa, P. A. Algarabel, C. Marquina, J. Blasco, J. García, S. Oseroff, and S.-W. Cheong, *Phys. Rev. B* **56**, 8902 (1997).
- <sup>34</sup>M. Eibschütz, S. Shtrikman, and D. Treves, *Phys. Rev.* **156**, 562 (1967).
- <sup>35</sup>P. C. Hohenberg and B. I. Halperin, *Rev. Mod. Phys.* **49**, 435 (1977).
- <sup>36</sup>S. Mukherjee, R. Ranganathan, P. S. Anilkumar, and P. A. Joy, *Phys. Rev. B* **54**, 9267 (1996).
- <sup>37</sup>M. Itoh, I. Natori, S. Kubota, and K. Motoya, *J. Phys. Soc. Jpn.* **63**, 1486 (1994).
- <sup>38</sup>R. S. Freitas, L. Ghivelder, F. Damay, F. Dias, and L. F. Cohen, *Phys. Rev. B* **64**, 144404 (2001).
- <sup>39</sup>X. J. Liu, Z. Q. Li, A. Yu, M. L. Liu, W. R. Li, B. L. Li, P. Wu, H. L. Bai, and E. Y. Jiang, *J. Magn. Magn. Mater.* **313**, 354 (2007).
- <sup>40</sup>L. Ghivelder, I. Abrego Castillo, M. A. Gusmão, J. A. Alonso, and L. F. Cohen, *Phys. Rev. B* **60**, 12184 (1999).
- <sup>41</sup>P. P. Vaishnava, U. Senaratne, E. C. Buc, R. Naik, V. M. Naik, G. M. Tsoi, and L. E. Wenger, *Phys. Rev. B* **76**, 024413 (2007).
- <sup>42</sup>T. D. Shen, R. B. Schwarz, and J. D. Thompson, *J. Appl. Phys.* **85**, 4110

(1999).

<sup>43</sup>C. P. Bean and J. D. Livingston, *J. Appl. Phys.* **30**, S120 (1959).

<sup>44</sup>A. Arrott, *Phys. Rev.* **108**, 1394 (1957).

<sup>45</sup>A. Aharoni, *J. Appl. Phys.* **56**, 3479 (1984).

<sup>46</sup>S. H. Kilcoyne, P. M. Bentley, and D. Greig, *J. Magn. Magn. Mater.* **272–276**, 1383 (2004).

<sup>47</sup>B. D. Cullity, *Introduction to Magnetic Materials* (Addison-Wesley, Philippines, 1972).

<sup>48</sup>K. De, M. Thakur, A. Manna, and S. Giri, *J. Appl. Phys.* **99**, 013908 (2006).

<sup>49</sup>X.-Y. Wang, L. Gan, S.-W. Zhang, and S. Gao, *Inorg. Chem.* **43**, 4615 (2004).